

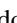
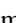



**Kittel law and domain formation mechanism in PbTiO<sub>3</sub>/SrTiO<sub>3</sub> superlattices**

Fernando Gómez-Ortiz <sup>1</sup>, Hugo Aramberri <sup>2</sup>, Juan M. López,<sup>3</sup> Pablo García-Fernández <sup>1</sup>,  
Jorge Íñiguez <sup>2,4</sup> and Javier Junquera <sup>1,\*</sup>

<sup>1</sup>*Departamento de Ciencias de la Tierra y Física de la Materia Condensada, Universidad de Cantabria, Avenida de los Castros, s/n, E-39005 Santander, Spain*

<sup>2</sup>*Materials Research and Technology Department, Luxembourg Institute of Science and Technology (LIST), Avenue des Hauts-Fourneaux 5, L-4362 Esch/Alzette, Luxembourg*

<sup>3</sup>*Instituto de Física de Cantabria (IFCA), Universidad de Cantabria-CSIC, E-39005 Santander, Spain*

<sup>4</sup>*Department of Physics and Materials Science, University of Luxembourg, Rue du Brill 41, L-4422 Belvaux, Luxembourg*



(Received 3 March 2023; accepted 26 April 2023; published 4 May 2023)

We report second-principles simulations on the structural and energetic properties of domains in (PbTiO<sub>3</sub>)<sub>n</sub>/(SrTiO<sub>3</sub>)<sub>n</sub> superlattices. For the explored layer thickness ( $n$  ranging between 8 and 16 unit cells) and lateral sizes of the domains, the most stable configuration corresponds to polar domains separated by a sequence of counter-rotating vortices (clockwise/counterclockwise) perpendicular to the stacking direction and acting as domain walls. The balance between the domain wall energy and the electrostatic energy yields to an optimal domain period  $\omega$  that is proportional to the square root of the thickness of the PbTiO<sub>3</sub> layer, following the Kittel law. For a given lateral size of the simulation box, suboptimal domain structures (with a width larger than the one predicted by the Kittel law) can be obtained in a metastable form. However, at finite temperature, molecular dynamics simulations show the spontaneous change of periodicity, which implies the formation of new domains whose generation is initiated by the nucleation of vortices and antivortices at the interface between the SrTiO<sub>3</sub> and the PbTiO<sub>3</sub> layers. The vortices progressively elongate and eventually annihilate with the antivortices yielding the formation of new domains to comply with the Kittel law via defect recombination.

DOI: [10.1103/PhysRevB.107.174102](https://doi.org/10.1103/PhysRevB.107.174102)

**I. INTRODUCTION**

A common feature among the family of ferroelectric materials is the formation of domain structures, regions of space with different polarizations separated by boundaries called domain walls [1,2]. Domains of opposite polarization lead to an overall charge neutrality at the surfaces reducing the depolarization field and the associated electrostatic energy.

The structure and energetics of domains in ferroic materials were first addressed by Landau and Lifshitz [3], and one decade later by Kittel [4,5] in his studies on ferromagnetic domains. The delicate balance between the energy of the boundary between domains, the magnetic field energy of the configuration, and the anisotropy energy of the spin orientation determine the relationship between the width of the domains,  $\omega$ , and the thickness of the material,  $d$  [4]. Adding up all the energy costs and minimizing this with respect to the domain size leads to a square-root dependence of  $\omega$  as a function of  $d$ . This is the so-called Landau-Kittel law,  $\frac{\omega^2}{\delta} = Ad$ , where  $A$  is an adimensional proportionality constant and  $\delta$  is the thickness of the domain wall. Although the earlier works assumed domain walls of zero width, it was later shown that the Kittel law was also valid at the Ginzburg-Landau level where finite width domain walls may form [6]. Here, we focus on this formula since it is closer to the case studied in the

present paper. This law was extended to ferroelectric materials by Mitsui and Furuichi [7] studying the domain structure of the Rochelle salt, where the electrostatic, elastic, and gradient energies determine the number and width of the domains for a given thickness of the material. The square-root dependence was further generalized under specific periodicities and screening conditions to the case of ultrathin ferroelectric layers [8] and to the case of superlattices with paraelectric materials [9]. Moreover, Roitburd expanded it also for ferroelastic thin films under epitaxial strain [10]. Therefore, it seems that the Landau-Kittel law of stripe domain width on film thickness is a general property of all ferroics [2].

Beyond the analytical derivations, the validity of the law has been confirmed by first-principles-based studies in ferroelectric [11] and multiferroic [12] thin films with thicknesses down to three unit cells. Following the spirit of these two works, we widen the applicability of the Kittel law to the case of ferroelectric/dielectric superlattices characterized by a ground state consisting of polar domains separated by a sequence of counter-rotating vortices (clockwise/counterclockwise) acting as domain walls [13–15]. Using second-principles simulations we validate the law for this complex polarization texture. Very interestingly, we show how when the system is initialized from a metastable state, where the density of domains is smaller than the one predicted by the Kittel law, it evolves upon heating to the ground state via defect recombination. The driving mechanism for the generation and closure of new domains is the recombination

\*Corresponding author: [javier.junquera@unican.es](mailto:javier.junquera@unican.es)

of vortex and antivortex defects generated at the interface between  $\text{PbTiO}_3$  and  $\text{SrTiO}_3$ .

## II. METHODOLOGY

The second-principles simulations were performed using the same methodology presented in previous works [16,17], as implemented in the SCALE-UP package [16,18]. The second-principles parameters of both materials were fitted from density functional theory imposing a hydrostatic pressure of  $-11.2$  GPa to counter the underestimation obtained by the local density approximation of the cubic lattice constant that was taken as the reference structure [19]. We imposed an epitaxial constraint assuming in-plane lattice constants of  $a = b = 3.901$  Å, forming an angle  $\gamma = 90^\circ$  mimicking the conditions of a  $\text{SrTiO}_3$  substrate. The interatomic potentials, and the approach to simulate the interface, are the ones first introduced in Ref. [17]. For a given value of supercell periodicity  $n$ ,  $(\text{PbTiO}_3)_n/(\text{SrTiO}_3)_n$ , several values of lateral size  $L$  were relaxed, making them commensurate with the number of simulated domains. We solved the models by running Monte-Carlo-simulated annealing from 60 K down to very low temperatures (0.003 K), typically comprising 20 000 relaxation sweeps. Regular Langevin molecular dynamics methods at a constant temperature of  $T = 90$  K were also used to solve the models in order to follow the dynamics of the emergent domains. For computational feasibility, we have focused on a simulation supercell made of a periodic repetition of  $L \times 1 \times 2n$  elemental perovskite unit cells for the Monte-Carlo-simulated annealings and of  $L \times 10 \times 2n$  for following the dynamics of the domains. As proven in Ref. [20], at low temperatures ( $T < 73$  K), the vortices do not vary along the axial  $y$  direction. Therefore, the simplification of taking one unit cell along this direction does not affect the validity of the model while it speeds up the calculations. However, when  $T = 90$  K a sufficiently high number of unit cells along the  $y$  direction must be considered in order to account for the variation along the axial direction.

We obtained the force-constant band calculations using the direct supercell approach as implemented in the PHONOPY package [21]. To this end, we considered the high-symmetry unit cell of the superlattices (in which the atoms in the  $\text{PbTiO}_3$  and  $\text{SrTiO}_3$  layers occupy the cubicle perovskite positions), and repeated it  $4 \times 4$  times in the  $xy$  plane to build the supercell for the calculations, which we found to be large enough to yield well-converged results. We included the nonanalytical contribution to the bands which accounts for the splitting between the longitudinal and transverse polar bands as implemented in Ref. [22].

Local polarizations are computed within a linear approximation of the product of the Born effective charge tensor times the atomic displacements from the reference structure positions divided by the volume of the unit cell.

## III. RESULTS

### A. Validation of Kittel law

We have checked the validity of the Kittel law in our superlattices following a similar recipe as in Refs. [11,12]. For different layer thicknesses  $n$  with constant and equal

dielectric/ferroelectric ratio, ranging between 8 and 16 unit cells (u.c.), the lateral size of the supercell to host two domains was optimized [see Fig. 1(a)]. In order to achieve this goal for every value of  $n$ , different lengths of the supercell along the  $x$  direction,  $L$ , were simulated. Once  $n$  and  $L$  were fixed, the initial atomic positions were chosen to mimic a couple of pure Ising domains, where the polarization changes abruptly from pointing upwards (up domain) to downwards (down domain) along the  $z$  direction in just one unit cell, as shown in Fig. 1(b). This configuration was taken as the starting point of the Monte Carlo annealing. The resulting typical dipole configuration, a local minimum at low temperature, is shown in Fig. 1(c). The spontaneous formation of alternating pairs of clockwise/counterclockwise vortices along the  $x$  direction is clearly visible, together with the development of an axial component of the polarization along the  $y$  direction. These vortices were already theoretically predicted from phenomenological theories [23,24], first-principles-based effective Hamiltonian [25], second-principles simulations [15,17,20], or full first-principles calculations [13], and experimentally demonstrated [14] in  $\text{PbTiO}_3/\text{SrTiO}_3$  superlattices. For a given layer thickness, the energy per five atom unit cell as a function of the lateral size of the supercell, always assuming the presence of two domains in the simulation box, is shown in Fig. 2(a). The first observation that can be drawn is that the larger the layer thickness  $n$ , the smaller the energy per unit cell. This fact stems from two different causes. On the one hand, the polarization in the  $\text{PbTiO}_3$  layers increases with  $n$ , tending to the bulk polarization value and approaching the ground state of the domain. On the other hand, the larger the layer thickness, the smaller the polarization within the  $\text{SrTiO}_3$  layer; the system undergoes a transition from an electrostatically “coupled” regime for small  $n$  to a “decoupled” regime for large  $n$  [6,26,27]. Since the  $\text{SrTiO}_3$  layers will be closer to the ground-state unpolarized configuration, the energy is also reduced. The second observation that can be drawn is that the energy curve of the two-domain structure as a function of the lateral size  $L$  presents a minimum corresponding to the most stable geometry. The larger the layer thickness, the shallower the minimum, that is localized for longer values of  $L$ . From these minima, we can infer the optimal width of the domain,  $\omega$ . Assuming that the domain wall is one unit cell thick [in good agreement with our simulations; see Fig. 1(c) for a typical case],  $\omega = L/2 - 1$  unit cells. Plotting the square of these optimal widths against the thickness of the  $\text{PbTiO}_3$  layer [red dots in Fig. 2(b)], we recover a linear behavior as predicted by the Kittel law, a tendency also shown in  $\text{BiFeO}_3$  [12] and  $\text{Pb}(\text{Zr}, \text{Ti})\text{O}_3$  ultrathin films [11].

Alternatively, one can try to predict the optimal width of the multidomain structure by studying force-constant bands such as the ones presented in Fig. 3(a). Following the unstable modes along  $\Gamma$ - $X$  we can identify  $q_{\min}$  as the wave vector associated with the strongest instability describing vortex structures as the ones presented in Fig. 3(b). From this value we can infer the optimal width as  $\omega = \frac{1}{2q} - 1$  [see the blue squares in Fig. 2(b)]. Interestingly, while the square-root dependence of the domain width as a function of the layer periodicity is nicely reproduced, there exists a discrepancy with the results obtained via the first method. The (harmonic) force-constant analysis predicts narrower domains than the ones obtained from a full energy minimization. This

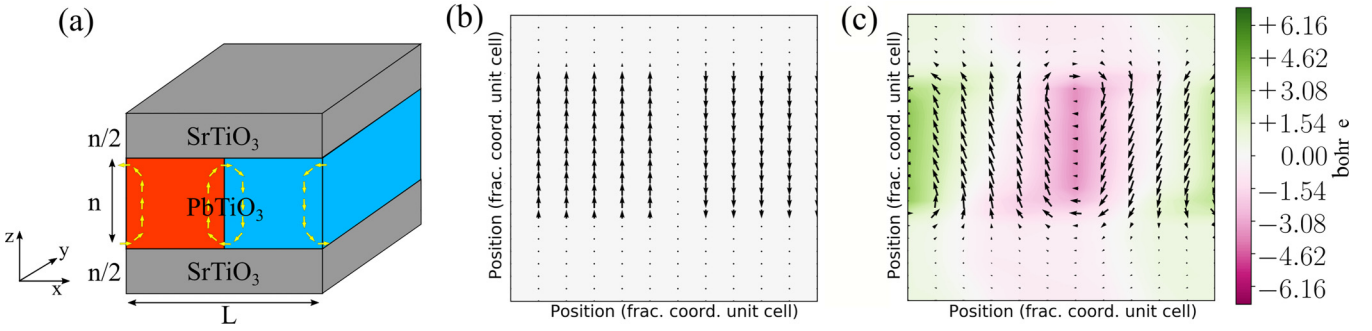


FIG. 1. Structural relaxation of a two-domain structure in  $(\text{PbTiO}_3)_n/(\text{SrTiO}_3)_n$  superlattices. (a) Schematic view of the simulation cell periodically repeated in the three directions of the space. Red (blue) regions indicate the positive (negative) polarization domains along the  $z$  direction. (b) Local dipoles of the initial Ising-like configuration presenting a clear two-domain structure for a layer thickness of  $n = 12$ , and a lateral size  $L = 12$  u.c. (c) Corresponding pattern of local dipoles after relaxation, showing an alternating clockwise/counterclockwise polar vortex configuration [15] along  $x$ . The domain wall thickness  $\delta$  extends over one unit cell. Colors represent the axial component of the polarization, perpendicular to the plane defined by the vortices.

difference must be due to anharmonic effects and/or the fact that the fully relaxed structures feature a combination of phonon mode distortions to optimize the energy. Thus, for example, the development of a slight offset coupled with an in-plane component of the polarization as the one shown in Fig. 1(c) and experimentally attained [14], although not captured in the force-constant analysis [see how vortices are centered in Fig. 3(b)], reduces the normal component of the polarization to the surface. The tilt of the polarization reduces the depolarization charges at the surface and allows the widening of the domains, resulting in the underestimate of the domain width predicted by the harmonic analysis.

We remind that our results have been obtained for a constant ratio between the number of unit cells of  $\text{SrTiO}_3$  and  $\text{PbTiO}_3$  equal to one. An analytical model for different ratios was studied in Ref. [9].

## B. Domain formation

Up to now, the existence of two domains in the simulation box has been imposed in the calculations. In the following we

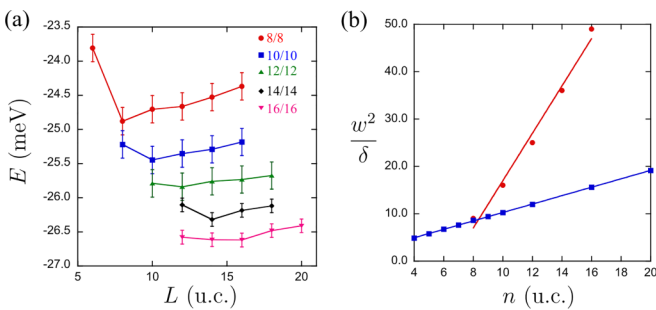


FIG. 2. Optimization of the lateral size of a two-domain structure in  $(\text{PbTiO}_3)_n/(\text{SrTiO}_3)_n$  superlattices. (a) Energy per five atom unit cell as a function of the lateral size of the supercell for different periodicities: red dots ( $n = 8$ ), blue squares ( $n = 10$ ), green uptriangles ( $n = 12$ ), black diamonds ( $n = 14$ ), and magenta downtriangles ( $n = 16$ ). (b) Linear fit of the squared optimized width of the domain as a function of the layer thickness by two procedures. Red dots correspond to minimizing the total energy of the supercell while blue squares correspond to the minimum of the force-constant bands along  $\Gamma$ -X. Here, u.c. stands for unit cell.

shall study the phase competition between different configurations under suboptimal domain widths. This is shown in Fig. 4 where we compare the energy per unit cell considering two or four domains for a given layer thickness  $n$  and lateral size of the supercell  $L$ . Again, for each pair of  $(n, L)$  a Monte Carlo annealing was carried out starting from purely  $180^\circ$  Ising-like structures containing two- or four-domain walls in the simulation box. In every case, the final relaxed structures display the typical polar vortex configuration, similar to the one shown in Fig. 1(c). In Fig. 4 we plot the evolution of the energy profile per five atom unit cell as a function of the lateral size of the supercell. As already discussed in Fig. 2(a), for a given amount of domain walls in the supercell, the larger the layer thickness  $n$ , the smaller the total energy. But the most important conclusion that can be drawn from Fig. 4 is that, for a given  $n$ , a crossover between the two- and four-domain configurations is found for a critical length  $L_c$ , whose value increases with  $n$ , as marked by the solid squares in Fig. 4. Studying lateral sizes far from the coexistence regions (below or above  $L_c$ ) different characteristic features can be observed for the evolution of the unstable phases. In Fig. 5 we show the behavior for a layer thickness of  $n = 12$ . Below  $L_c$  (short lateral sizes) the four-domain structure is only metastable since the large penalty coming from the gradient energy term is not compensated by the saving in electrostatic energy. Indeed, in this metastable regime the system tends to reduce the energy gradient contribution by forming polarization waves [28] [Fig. 5(a)] along the  $[100]_{\text{pc}}$  direction, with the concomitant onset of a net in-plane polarization, and the displacement of the center of the vortices in the  $\text{PbTiO}_3$  layer towards the interface with  $\text{SrTiO}_3$ . The smaller the lateral size of the supercell  $L$ , the larger the offset between neighboring vortex cores that do not fit in the center of the  $\text{PbTiO}_3$  layer as in the case of larger lateral sizes [see Fig. 5(d)]. This phenomenon has also been observed in  $\text{BiFeO}_3$  ultrathin films [12].

The energetically most favorable configuration presents only two domains [Fig. 5(c)], with larger domain sizes and a smaller number of domain walls. However, the energy of this configuration increases with  $L$ . Above  $L_c$  (long lateral sizes), the two-domain structure [Fig. 5(d)] becomes metastable since the electrostatic energy penalty starts to grow and become dominant. Therefore, we observe new patterns

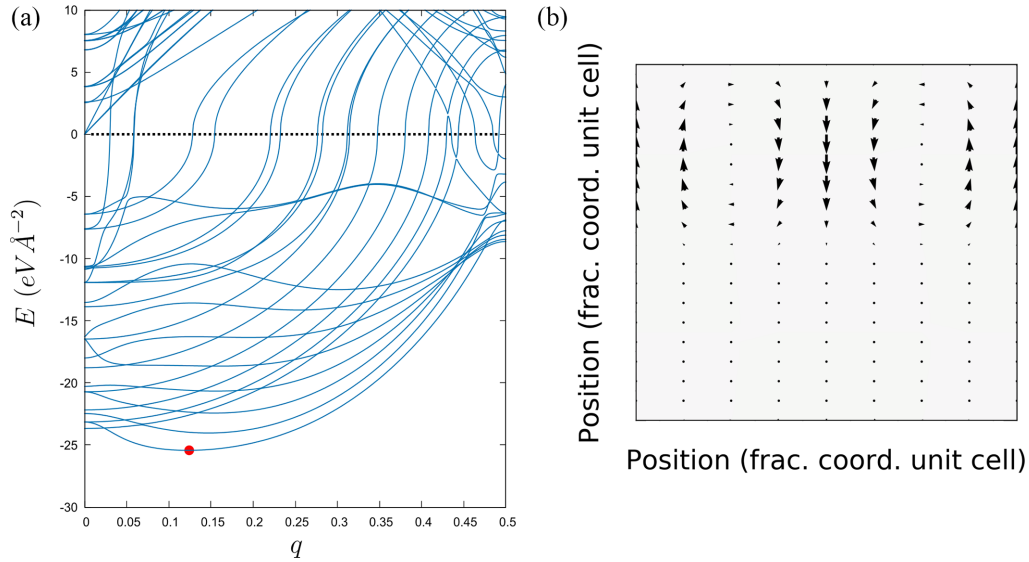


FIG. 3. (a) Force-constant bands along  $\Gamma$ -X obtained after diagonalization of the force-constant matrix in a  $(\text{PbTiO}_3)_9/(\text{SrTiO}_3)_9$  supercell. The dashed line indicates the energy of the centrosymmetric configuration which is taken as the reference. The red dot indicates the position of the strongest instability located at  $q_{\min} = 0.123$  in fractional units. (b) Relaxed structure following the strongest instability of the force-constant bands.

containing two vortices and two antivortices at the interface with  $\text{SrTiO}_3$ , as will be further discussed in Fig. 6. Indeed, increasing the temperature we observe how the system is able to escape from this metastable configuration and transit to a state with four domains, as shown in Fig. 5(b). The new vortices formed at the interface between  $\text{PbTiO}_3$  and  $\text{SrTiO}_3$  layers, shown in Fig. 5(d), serve as nucleation points of new down (respectively, up) domains dividing the already existing

up (respectively, down) polarization regions. The formation of these new domains reduces the polarization charges generated at the interface.

Assuming in our simulations the in-plane lattice constant of  $\text{SrTiO}_3$  [15], and at low-enough temperatures ( $T < 50$  K), this state is a long-lived metastable phase. The new vortex defects formed at the interface are not able to propagate and close the new domain. Increasing the temperature (beyond 90 K), or inducing compressive strain (beyond  $-0.5\%$ ) on the sample, the energy barrier can be overcome and we observe the formation of new domains. Interestingly, the transition

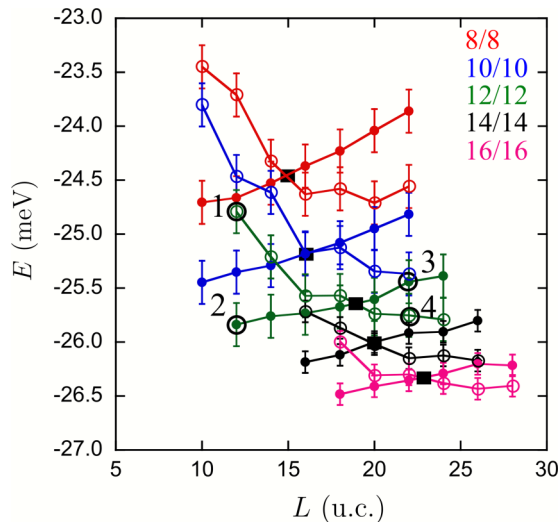


FIG. 4. Energy profile per five atom unit cell as a function of the lateral size of the supercell for the two- (solid dots) and four- (open dots) domain structures. Different layer thicknesses are indicated by colors: red ( $n = 8$ ), blue ( $n = 10$ ), green ( $n = 12$ ), black ( $n = 14$ ), and magenta ( $n = 16$ ). Solid black squares indicate the crossing point where the four-domain structure becomes more stable. Numbers 1–4 label the different dipole patterns plotted in Fig. 5. Here, u.c. stands for unit cell.

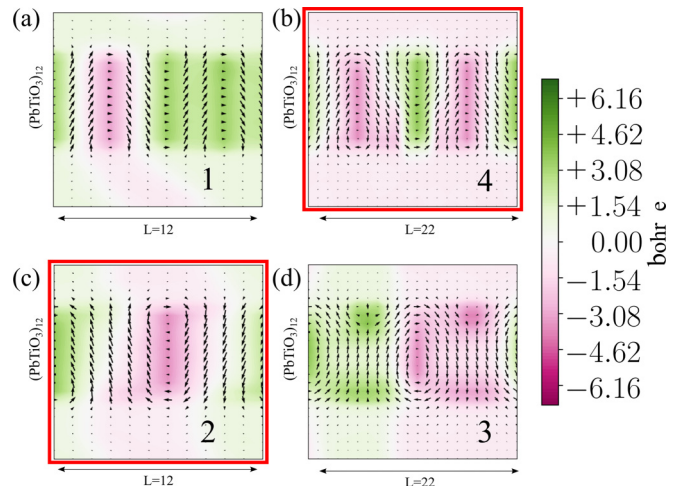


FIG. 5. Polarization map of the relaxed structures labeled from 1 to 4 in Fig. 4 for different lateral sizes  $L$  and a layer thickness of  $n = 12$ . Black arrows indicate the local dipoles, projected onto the  $(x, y)$  plane. The axial component of the polarization along the  $[010]_{\text{pc}}$  direction is represented by the green and magenta color map. Units of the dipoles in  $e \times \text{bohr}$ , where  $e$  is the electron charge. Red squares highlight the most stable structure for each lateral size.



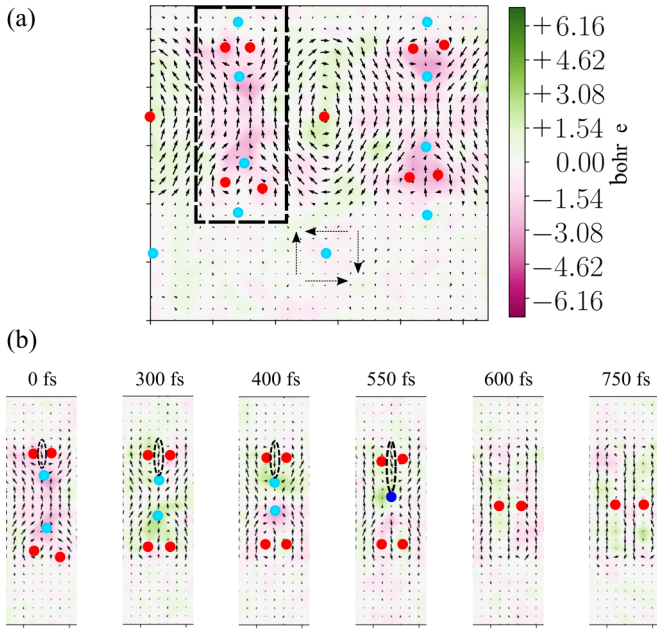


FIG. 6. Polarization map for a  $n = 14$ ,  $L = 28$  supercell at finite temperature ( $T = 90$  K) and compressive epitaxial strain of  $-0.5\%$ . (a) Initial two-domain structure configuration. The dashed square delimits the upwards domain studied for the dynamics in (b), where the dashed arrows within the  $\text{SrTiO}_3$  are a guide to the eye to locate one of the different antivortex structures. (b) Temporal evolution obtained by molecular dynamics simulations at finite temperature. Red dots indicate the location of the vortex while light- and dark-blue dots indicate the location of antivortices of vorticity  $-1$  and  $-2$ , respectively. Meaning of the arrows and colors as in Fig. 5.

to the optimal domain configuration is not observed at high domain densities. Below  $L_c$  the system is trapped in a polarization wave and cannot transit to a lower-density domain configuration by means of increasing temperature. This asymmetry comes as a consequence of the different nature between the electrostatic and gradient energy penalties.

Molecular dynamics simulations at constant temperature show how the recombination of vortex-antivortex pairs is the driving mechanism for the domain propagation through the sample until the new domain is completely formed. In Fig. 6(a) we show in detail the case of  $n = 14$ ,  $L = 28$  at a constant temperature  $T = 90$  K and a slight compressive strain of  $-0.5\%$ . There we can notice the balance of vortex and antivortex defects resulting in a zero net vorticity on the supercell as stated by the Poincaré-Hopf theorem for our specific periodic boundary conditions. The antivortex textures are mostly formed at the  $\text{SrTiO}_3$  layers where the magnitude of the polarization and the concomitant electrostatic energy of head-to-head and tail-to-tail domains is smaller. This is in accordance with first-principles calculations [13].

In Fig. 6(b) we analyze the time evolution of a portion within the up domain of the same superlattice [see the dashed square in Fig. 6(a)], in a region where new polarization vortices have been formed at the interfaces between the  $\text{PbTiO}_3$  and the  $\text{SrTiO}_3$  layers. The presence of two vortices (red circles) and an antivortex (light-blue circle) is clearly observed both at the top and the bottom interface. Starting from

this configuration these vortices and antivortices change their shapes in order to reduce the total energy of the system. First, the vortices elongate, while keeping their centers essentially at the same positions. This comes with two main consequences. First, locally, the number of unit cells with down polarization increases with time [from three at the initial configuration to four at 300 or 400 fs, or even five at 550 fs; see the dashed ovals at Fig. 6(b)]. Second, the region where the local polarization points in plane to close the vortices moves towards the center of the  $\text{PbTiO}_3$  layer, and so does the center of the antivortices. At 550 fs, the two antivortices merge to form an antivortex with vorticity  $-2$  at the center of the  $\text{PbTiO}_3$  layer [dark-blue point in Fig. 6(b)]. The field disturbance doubles its charge with a high energetic cost [in accordance with the Kosterlitz-Thouless analysis in the sample XY model [29,30], where the energy of the vortices increases (quadratically) with the vorticity]. This is the reason why this state is very short lived in the molecular dynamic simulations. Only 50 fs later, it annihilates with two vortices. In this process a new domain with down polarization is formed, together with two new elongated clockwise/counterclockwise pairs. Finally, the new domain widens until recovering the optimal lateral size determined by the Kittel law.

#### IV. CONCLUSIONS

In summary, we theoretically extend the application of the Kittel law to the polar vortex phase in  $(\text{PbTiO}_3)_n/(\text{SrTiO}_3)_n$  superlattices. For the explored layer thicknesses, the square-root dependence of the domain period with the thickness of  $\text{PbTiO}_3$  is restored by two different procedures: (i) full minimization of the energy where all possible interactions are considered, and (ii) analyzing the harmonic force-constant bands. We find that the harmonic approach predicts narrower domains, which is consistent with the fact that anharmonic effects, such as the development of an offset, tend to reduce the depolarizing fields on the structure.

Moreover, studying the phase competition under suboptimal domain widths we showed how at low-domain density new domains can be formed to relax electrostatic constraint. These domains nucleate as vortex/antivortex pair defects at the interfaces with  $\text{SrTiO}_3$  and propagate through the lattice by means of recombination until the new domains are completely formed. This recombination of vortex/antivortex is driven by the high-energy costs of polarization patterns containing vortex/antivortex pairs.

#### ACKNOWLEDGMENTS

F.G.-O., P.G.-F., and J.J. acknowledge financial support from Grant No. PGC2018-096955-B-C41 funded by MCIN/AEI/10.13039/501100011033 and by ERDF “A way of making Europe” by the European Union. F.G.-O. acknowledges financial support from Grant No. FPU18/04661 funded by MCIN/AEI/10.13039/501100011033. J.M.L. was supported by Grant No. PID2021-125543NB-I00 funded by MCIN/AEI/10.13039/501100011033/ and by ERDF “A way of making Europe” by the European Union. H.A. and J.I. were funded by the Luxembourg National Research Fund through Grant No. C21/MS/15799044/FERRODYNAMICS. The

authors thankfully acknowledge computing time at Altamira supercomputer and the technical support provided by the Instituto de Física de Cantabria (IFCA) and Universidad de Cantabria (UC). The authors would also like to thank

J. Á. Herrero for his valuable assistance with the supercomputing environment HPC/HTC cluster “Calderon,” supported by datacenter 3Mares, from Universidad de Cantabria.

- 
- [1] A. K. Tagantsev, L. E. Cross, and J. Fousek, *Domains in Ferroic Crystals and Thin Films* (Springer, New York, 2010).
- [2] G. Catalan, J. Seidel, R. Ramesh, and J. F. Scott, Domain wall nanoelectronics, *Rev. Mod. Phys.* **84**, 119 (2012).
- [3] L. Landau and E. Lifshitz, On the theory of the dispersion magnetic permeability in ferromagnetic bodies, *Phys. Z. Sowjetunion* **8**, 153 (1935).
- [4] C. Kittel, Theory of the structure of ferromagnetic domains in films and small particles, *Phys. Rev.* **70**, 965 (1946).
- [5] C. Kittel, Physical theory of ferromagnetic domains, *Rev. Mod. Phys.* **21**, 541 (1949).
- [6] V. A. Stephanovich, I. A. Luk'yanchuk, and M. G. Karkut, Domain-Enhanced Interlayer Coupling in Ferroelectric/Paraelectric Superlattices, *Phys. Rev. Lett.* **94**, 047601 (2005).
- [7] T. Mitsui and J. Furuichi, Domain structure of Rochelle salt and  $\text{KH}_2\text{PO}_4$ , *Phys. Rev.* **90**, 193 (1953).
- [8] G. Catalan, H. Béa, S. Fusil, M. Bibes, P. Paruch, A. Barthélémy, and J. F. Scott, Fractal Dimension and Size Scaling of Domains in Thin Films of Multiferroic  $\text{BiFeO}_3$ , *Phys. Rev. Lett.* **100**, 027602 (2008).
- [9] D. Bennett, M. Muñoz Basagoiti, and E. Artacho, Electrostatics and domains in ferroelectric superlattices, *R. Soc. Open Sci.* **7**, 201270 (2020).
- [10] A. L. Roitburd, Equilibrium structure of epitaxial layers, *Phys. Status Solidi A* **37**, 329 (1976).
- [11] B.-K. Lai, I. Ponomareva, I. Kornev, L. Bellaiche, and G. Salamo, Thickness dependency of  $180^\circ$  stripe domains in ferroelectric ultrathin films: A first-principles-based study, *Appl. Phys. Lett.* **91**, 152909 (2007).
- [12] S. Prosandeev, S. Lisenkov, and L. Bellaiche, Kittel Law in  $\text{BiFeO}_3$  Ultrathin Films: A First-Principles-Based Study, *Phys. Rev. Lett.* **105**, 147603 (2010).
- [13] P. Aguado-Puente and J. Junquera, Structural and energetic properties of domains in  $\text{PbTiO}_3/\text{SrTiO}_3$  superlattices from first principles, *Phys. Rev. B* **85**, 184105 (2012).
- [14] A. K. Yadav, C. T. Nelson, S. L. Hsu, Z. Hong, J. D. Clarkson, C. M. Schlepütz, A. R. Damodaran, P. Shafer, E. Arenholz, L. R. Dedon, D. Chen, A. Vishwanath, A. M. Minor, L. Q. Chen, J. F. Scott, L. W. Martin, and R. Ramesh, Observation of polar vortices in oxide superlattices, *Nature (London)* **530**, 198 (2016).
- [15] P. Shafer, P. García-Fernández, P. Aguado-Puente, A. R. Damodaran, A. K. Yadav, C. T. Nelson, S.-L. Hsu, J. C. Wojdeł, J. Íñiguez, L. W. Martin, E. Arenholz, J. Junquera, and R. Ramesh, Emergent chirality in the electric polarization texture of titanate superlattices, *Proc. Natl. Acad. Sci. USA* **115**, 915 (2018).
- [16] J. C. Wojdeł, P. Hermet, M. Ljunberg, P. Ghosez, and J. Íñiguez, First-principles model potentials for lattice-dynamical studies: general methodology and example of application to ferroic perovskite oxides, *J. Phys.: Condens. Matter* **25**, 305401 (2013).
- [17] P. Zubko, J. C. Wojdeł, M. Hadjimichael, S. Fernandez-Pena, A. Sené, I. Luk'yanchuk, J.-M. Triscone, and J. Íñiguez, Negative capacitance in multidomain ferroelectric superlattices, *Nature (London)* **534**, 524 (2016).
- [18] P. García-Fernández, J. C. Wojdeł, J. Íñiguez, and J. Junquera, Second-principles method for materials simulations including electron and lattice degrees of freedom, *Phys. Rev. B* **93**, 195137 (2016).
- [19] The bulk models are those of Ref. [16]; an interested reader should request them from the authors of that article.
- [20] F. Gómez-Ortiz, P. García-Fernández, J. M. López, and J. Junquera, Melting of crystals of polarization vortices and chiral phase transitions in oxide superlattices, *Phys. Rev. B* **105**, L220103 (2022).
- [21] A. Togo and I. Tanaka, First principles phonon calculations in materials science, *Scr. Mater.* **108**, 1 (2015).
- [22] X. Gonze and C. Lee, Dynamical matrices, born effective charges, dielectric permittivity tensors, and interatomic force constants from density-functional perturbation theory, *Phys. Rev. B* **55**, 10355 (1997).
- [23] G. B. Stephenson and K. R. Elder, Theory for equilibrium  $180^\circ$  stripe domains in  $\text{PbTiO}_3$  films, *J. Appl. Phys.* **100**, 051601 (2006).
- [24] A. M. Bratkovsky and A. P. Levanyuk, Continuous theory of ferroelectric states in ultrathin films with real electrodes, *J. Comput. Theor. Nanosci.* **6**, 465 (2009).
- [25] I. Kornev, H. Fu, and L. Bellaiche, Ultrathin Films of Ferroelectric Solid Solutions under a Residual Depolarizing Field, *Phys. Rev. Lett.* **93**, 196104 (2004).
- [26] V. A. Stephanovich, I. A. Luk'yanchuk, and M. G. Karkut, Domain proximity and ferroelectric transition in ferro-paraelectric superlattices, *Ferroelectrics* **291**, 169 (2003).
- [27] P. Zubko, N. Jecklin, A. Torres-Pardo, P. Aguado-Puente, A. Gloter, C. Lichtensteiger, J. Junquera, O. Stéphan, and J.-M. Triscone, Electrostatic coupling and local structural distortions at interfaces in ferroelectric/paraelectric superlattices, *Nano Lett.* **12**, 2846 (2012).
- [28] L. Lu, Y. Nahas, M. Liu, H. Du, Z. Jiang, S. Ren, D. Wang, L. Jin, S. Prokhorenko, C.-L. Jia, and L. Bellaiche, Topological Defects with Distinct Dipole Configurations in  $\text{PbTiO}_3/\text{SrTiO}_3$  Multilayer Films, *Phys. Rev. Lett.* **120**, 177601 (2018).
- [29] J. M. Kosterlitz and D. J. Thouless, Ordering, metastability and phase transitions in two-dimensional systems, *J. Phys. C: Solid State Phys.* **6**, 1181 (1973).
- [30] J. M. Kosterlitz, The critical properties of the two-dimensional XY model, *J. Phys. C: Solid State Phys.* **7**, 1046 (1974).